# Neutrino Geoscience

*Livia Ludhova*

IKP-2 Forschungzentrum Jülich, 52428 Jülich, Germany
RWTH Aachen University, 52062 Aachen, Germany

**DOI:** http://dx.doi.org/10.3204/DESY-PROC-2016-05/7

Neutrino geoscience is a newly born interdisciplinary field having as its main aim determination of the Earth's radiogenic heat through measurement of geoneutrinos: antineutrinos released in decays of long-lived radioactive elements inside the Earth. In fact, such measurements are a unique direct way how to pin-down this key element for many geophysical and geochemical Earth's models. The large–volume liquid scintillator detectors, originally built to measure neutrinos or anti-neutrinos from other sources, are capable to detect geoneutrinos, as it was demonstrated by KamLAND (Japan) and Borexino (Italy) experiments. Several future projects as SNO+ or JUNO have geoneutrino measurements among their scientific goals. This work covers the status-of-art of this new field, summarising its potential in terms of geoscience, the status of existing experimental results, and future prospects.

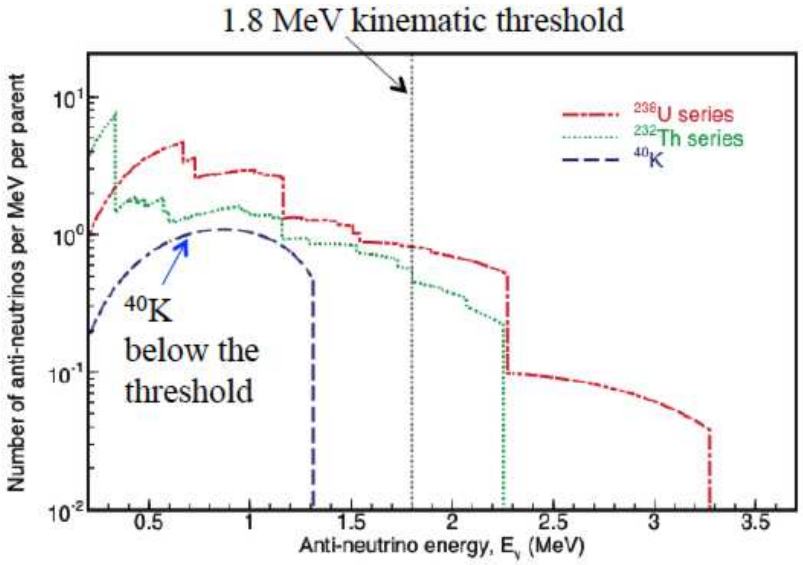


Figure 1: Energy spectrum of geoneutrinos. The dashed vertical line shows the energy threshold of the IBD interaction: currently the only detection method for geoneutrinos.

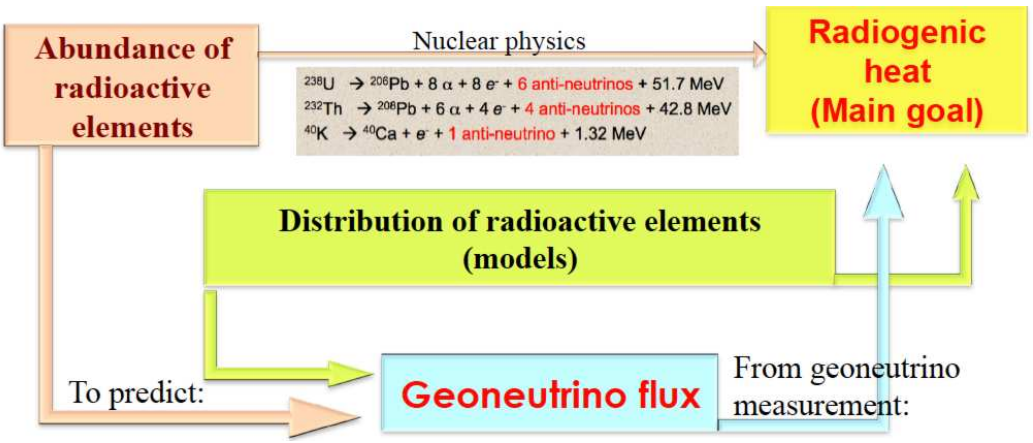


Figure 2: Schematic visualisation of the relations among the abundances and distributions of radioactive elements inside the Earth, the geoneutrino flux, and the radiogenic heat, the ultimate goal of geoneutrino measurements.

## 1 What are geoneutrinos and the main goal

Geoneutrinos are electron-flavour antineutrinos emitted in the $\beta$ decays of long-lived radioactive elements, called also *the heat producing elements* (HPE). Geoneutrinos are emitted along the decay chains of $^{238}$U and $^{232}$Th and in the $^{40}$K decay:

$$^{238}\mathrm{U} \rightarrow^{206} \mathrm{Pb} + 8\alpha + 8e^- + 6\bar{\nu}_e + 51.7 \quad \mathrm{MeV}, \tag{1}$$

$$^{232}\mathrm{Th} \rightarrow^{208} \mathrm{Pb} + 6\alpha + 4e^- + 4\bar{\nu}_e + 42.7 \ \mathrm{MeV}, \tag{2}$$

$$^{40}\mathrm{K} \rightarrow^{40} \mathrm{Ca} + e^- + \bar{\nu}_e + 1.31 \ \mathrm{MeV} \ (\mathrm{BR}\ 89.3\%). \tag{3}$$

Geoneutrino spectrum is shown in Fig. 1. Geoneutrinos are detected by the so called Inverse Beta Decay (IBD) interaction:

$$\bar{\nu}_e + p \rightarrow e^+ + n. \tag{4}$$

Due to the 1.8 MeV kinematic threshold of this reaction, only the high-energy tail of $^{238}$U and $^{232}$Th geoneutrinos can be detected, while all $^{40}$K geoneutrinos are below the threshold.

The main aim of geoneutrino studies is to determine the Earth's radiogenic heat, especially the unknown contribution from the mantle. The mantle composition is quite unknown with respect to the better-known crustal composition. Knowing the mass/abundances of HPE, the radiogenic heat is directly determined. The geoneutrino studies are, however, complicated through an unknown distribution of HPE, on which depends both the geoneutrino signal prediction as well as the final interpretation of the measured geoneutrino flux, see Fig. 2. Due to this, a close collaboration between neutrino physicists and geoscientists is strongly required in order to exploit the potential of geoneutrinos to its maximum.

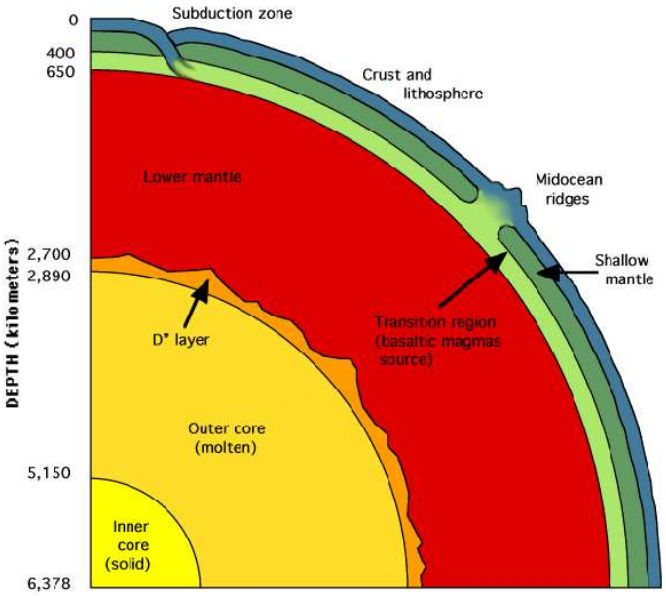


Figure 3: A schematic profile of the Earth structure (from http://www.homepages.ucl.ac.uk/ ucfbdxa/resint.htm).

## 2 The Earth and GeoSciences

The Earth was created in the process of accretion from undifferentiated material, to which chondritic meteorites are believed to be the closest in composition and structure. The bodies with a sufficient mass undergo the process of differentiation, e. g., a transformation from an homogeneous object into a body with a layered structure. The metallic core (3500 km radius) was the first to separate from the silicate primordial mantle, which further differentiated into the current mantle (3000 km thickness) and the crust (5 to 75 km). The Fe–Ni metallic core with up to ∼10% admixture of lighter elements, has a temperatures range from 4100 to 5800 K. Its central part, inner core with the radius ∼1300 km is solid due to high pressure. The 2200 km thick outer core is liquid and has a key role in the geo–dynamo process generating the Earth's magnetic field. The D″ layer is a core–mantle boundary, a 200 km thick seismic discontinuity of unclear origin. The lower mantle (2000 km) with a temperature gradient from 600 to 3700 K is solid, but viscose on long time scales. It is involved in the convection driving the movement of tectonic plates with a speed of a few centimetres per year. A transition zone in the depth of 400 - 600 km is a seismic discontinuity due to mineral recrystallisation. The upper mantle contains viscose asthenosphere on which are floating the lithospheric tectonic plates. These comprise the uppermost, rigid part of the mantle and the crust of two types: oceanic and continental. The continental crust (30 km average thickness) has the most complex history being the most differentiated and heterogeneous, consisting of igneous, metamorphic, and sedimentary rocks. The oceanic crust (5 - 10 km) is created along the mid–oceanic ridges, where the basaltic magma differentiates from the partially melting mantle. A schematic profile of the Earth structure can be found in Fig. 3.

The HPE are so called refractory, lithophile elements: they bound to the lighter partially melted liquid, leaving behind the HPE-depleted solid and denser residuum. Due to this mechanism, the HPE are strongly concentrated in the most complex continental crust (at the level of few ppm in average) and present in sub-ppm concentrations in the oceanic crust. The HPE concentration in the mantle is suppressed by few orders of magnitude and largely unknown. Due to the chemical affinity to silicates, no HPE are expected to be present in the metallic core.

How do we get information about the deep Earth? Seismology studies the propagation of the S and P seismic waves, providing the velocity and density profiles of the Earth. Geochemistry studies the chemical composition of the Earth. The depth of accessible rock samples is limited to the upper mantle. The global composition of the Bulk Silicate Earth (BSE) is derived through geochemical modelling, considering the correlations in isotopic abundances in the solar photosphere and in meteorites, as well as composition of the present day rocks. These BSE models describe the composition of the Primitive Mantle, the Earth composition after the core separation and before the crust-mantle differentiation. The estimates of the composition of the present-day mantle can be derived as a difference between the mass abundances predicted by the BSE models in the Primitive Mantle and those observed in the present crust. In this way, the predictions of the U and Th mass abundances in the mantle are made. An overview of different BSE models can be found for example in Šrámek et al. [1].

The Earth's surface heat flux is estimated based on the measurements of temperature gradients along several thousands of drill holes around the globe. The most recent evaluation of these data leads to the prediction of $47 \pm 2$ TW predicted by Davies and Davies (2010) [2], consistent with the estimation of Jaupart et al. (2007) [3]. The relative contribution of the radiogenic heat from radioactive decays to this flux is not known and this is the key information which can be pinned down by the geo-neutrino measurements. The geochemical, cosmochemical, and geodynamical models predict the radiogenic heat of $20 \pm 4$, $11 \pm 2$, and $33 \pm 3$ TW, respectively [1]. The crustal radiogenic power was recently evaluated by Huang et al. [4] as $6.8^{+1.4}_{-1.1}$ TW. By subtracting this contribution from the total radiogenic heat predicted by different BSE models, the mantle radiogenic power can be as little as 3 TW and as much as 23 TW. To determine this mantle contribution is one of the main goals and potentials of Neutrino Geoscience.

## 3 Geoneutrino detection

Geoneutrinos are detected by the large–volume liquid scintillator detectors placed in underground laboratories, in order to shield them from the cosmic radiation. The target for the IBD detection interaction shown in Eq. 4 are hydrogen nuclei from the hydrocarbon molecules of organic liquid scintillator. In this process, a positron and a neutron are emitted as reaction products. The positron promptly comes to rest and annihilates emitting two 511 keV $\gamma$-rays, yielding a *prompt event*, with a visible energy $E_{prompt}$, directly correlated with the incident antineutrino energy $E_{\bar{\nu}_e}$:

$$E_{prompt} = E_{\bar{\nu}_e} - 0.784 \text{ MeV}. \tag{5}$$

The emitted neutron keeps initially the information about the $\bar{\nu}_e$ direction, but is typically captured on protons only after quite a long time ($\tau$ = 200 - 250 $\mu$s, depending on scintillator), during which the directionality memory is lost in many scattering collisions. When the thermalised neutron is captured on proton, it gives a typical 2.22 MeV de-excitation $\gamma$-ray, which provides a coincident *delayed event*. The pairs of time and spatial coincidences between the

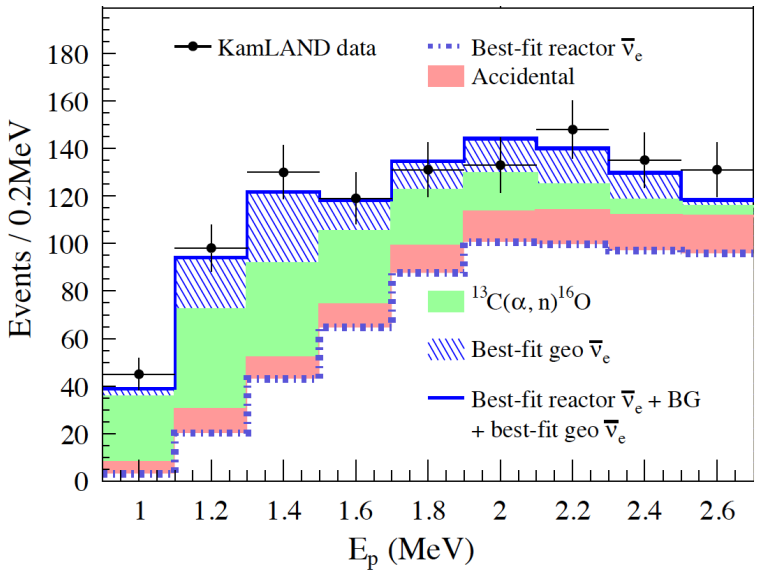


Figure 4: KamLAND prompt energy spectrum of $\bar{\nu}_e$ events in the geoneutrino energy region. Data together with the best-fit background and geo contributions are shown. Taken from [8].

prompt and the delayed signals offer a clean signature of $\bar{\nu}_e$ interactions, very different from the $\nu_e$ scattering process used in the neutrino detection.

For a ∼3 MeV antineutrino, the oscillation length is of ∼100 km, small with respect to the Earth's radius of ∼6371 km: the effect of the neutrino oscillation to the total neutrino flux is well averaged. Considering also the local matter effects [5], the net effect of flavour oscillations during the geo-neutrino propagation through the Earth is the average electron flavour survival probability of ∼0.55 with a very small spectral distortion, negligible for the precision of the current geo-neutrino experiments.

Typically, for the experimental sites built at the continental crust, about half of the total geoneutrino signal comes from the local crust in the area of few hundreds of kilometers around the detector [4]. In order to extract the mantle contribution from the measured geoneutrino signal, it is necessary to be able to subtract the crustal contribution. This means, that the local geology in the area of the experiment has to be known.

## 4 Latest geoneutrino measurements

Today, only two experiments succeeded to measure geoneutrinos: KamLAND [6, 7, 8] in Kamioka mine in Japan and Borexino [9, 10, 11] in Gran Sasso underground laboratory in Italy. KamLAND is a 1 kton liquid scintillator detector dedicated to the measurement of reactor antineutrinos, which provided one of the first proves of the existence of the phenomenon of neutrino oscillations and the most precise measurement of the $\Delta m^2_{12}$ mass splitting [12]. Borexino is 280 ton liquid scintillator detector, originally built to measure low-energy (below 1 MeV) solar neutrinos by means of elastic scattering off electrons. In contrast to IBD interac-

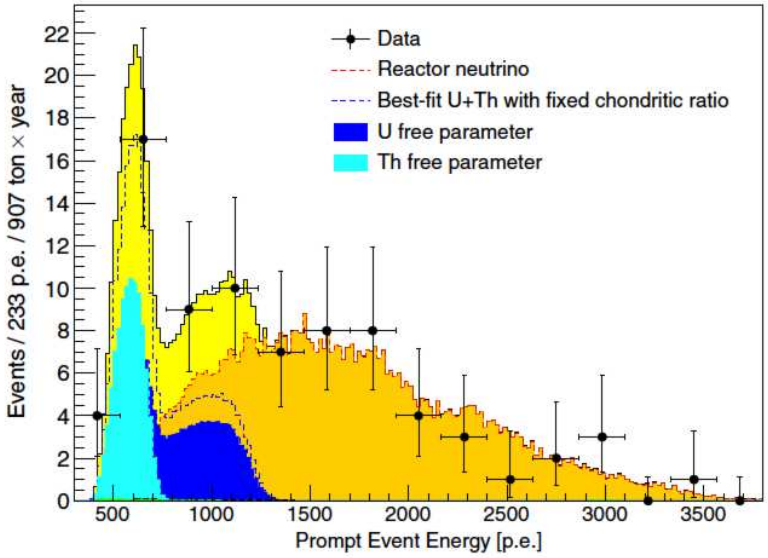


Figure 5: Prompt light yield spectrum in photoelectrons (p.e.) of 77 antineutrino candidates measured by Borexino and the best fit. 1 MeV corresponds to ∼500 p.e. Taken from [11].

tions (delayed coincidences), the measurement of singles puts more stringent requirements on the detector radio-purity. Borexino detector reached extremely high levels of radio-purity and produced unique results in solar neutrino spectroscopy [13]. Borexino geoneutrino measurement is almost free of non-antineutrino background components, as random coincidences, ($\alpha$, n) interactions and cosmogenic events. In addition, no nuclear power plants are in operation in Italy, further reducing the background for geoneutrino measurement.

The latest KamLAND result, $116^{+28}_{-27}$ geoneutrinos detected with $4.9 \times 10^{32}$ target-proton × year exposure, is from 2013 [8], including the period of low reactor antineutrino background after the April 2011 Fukushima disaster. The measured signal is in agreement with expectations, slightly disfavouring the geodynamical BSE models. The contribution of the local crust to the total geoneutrino signal was studied in [5, 14].

The new Borexino update from 2015 [11] is shown in Fig. 5. Within the exposure of $(5.5 \pm 0.3) \times 10^{31}$ target-proton × year, $23.7^{+6.5}_{-5.7}(\text{stat})^{+0.9}_{-0.6}(\text{sys})$ geoneutrino events have been detected. The null observation of geoneutrinos has a probability of $3.6 \times 10^{-9}$ ($5.9\sigma$). The contribution of the local crust to the total signal was studied in [15]. A geoneutrino signal from the mantle is confirmed at 98% confidence level. The radiogenic heat production for U and Th from the present best-fit result is restricted to the range 23 to 36 TW, taking into account the uncertainty on the distribution of HPE inside the Earth.

## 5 Future prospects

In the near future, a possible update is expected from KamLAND, including more data with low reactor antineutrino background. Borexino geoneutrino data-set will naturally end with the

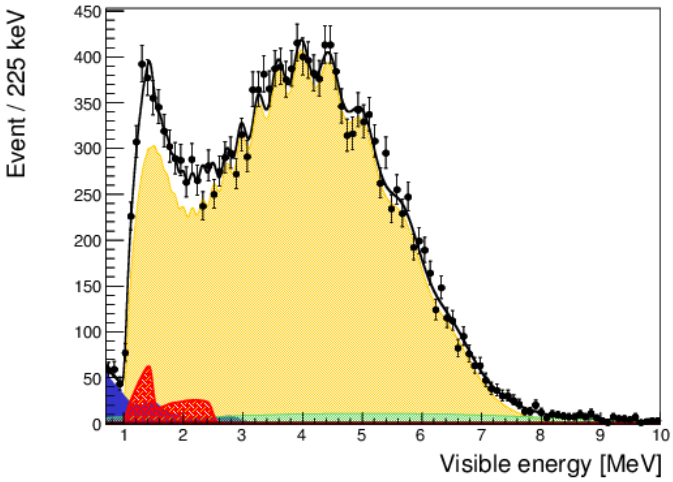


Figure 6: Example of a toy Monte Carlo for a possible 1-year geoneutrino measurement of JUNO. The different spectral components are shown as they result from the fit; black line shows the total sum for the best fit. The geoneutrino signal with Th/U fixed to chondritic ratio is shown in red. The following colour code applies to the backgrounds: orange (reactor antineutrinos), green ($^{9}$Li - $^{8}$He), blue (accidental), small magenta ($\alpha$, n). Taken from [17].

start of the SOX project at the end of 2017. Placing the strong $^{144}$Ce-$^{144}$Pr antineutrino source below the detector (in order to search for a hypothetical 1 eV$^2$ sterile neutrino), will make it impossible to measure geoneutrinos with its low rate of about 1 event every 2-3 months.

From the future projects, the SNO+ experiment, 1 kton liquid scintillator detector in Sudbury mine in Canada, should start its data taking soon, having geoneutrinos among its goals. This is also the case of 50 kton liquid scintillator detector JUNO in Jiangmen, China, which will start its data taking in 2020, towards determination of the neutrino mass hierarchy by measurement of reactor antineutrinos with 53 km baseline. Inevitable disadvantage of the large reactor antineutrino background and a relatively shallow depth, are both balanced by the detector large size and an excellent energy resolution of 3% at 1 MeV. The expected number of geoneutrino events is about 400/year [16]. Figure 6 demonstrates a possible measurement after 1 full year of data taking with the expected level of backgrounds [17]. Within the first years, JUNO geoneutrino measurement can quickly exceed the precision of current geoneutrino results.

A real breakthrough in this field would come with the proposed Hanohano [18] project in Hawaii, a 10 kton movable detector placed underwater. Geological setting on the HPE-depleted oceanic crust is an ideal location: the mantle contribution to the total geoneutrino flux would be dominant and the principal goal of the geoneutrino measurements, determination of the mantle signal, could be reached without the complication of the subtraction of the signal from the local continental crust.

In conclusion it can be said, that the new field of Neutrino Geoscience has been born and an inter-disciplinary community of physicists and geoscientists if developing. The first geoneutrino

results confirm the feasibility of these measurements. The measured rates are in agreement with the expectations, confirming that at this level of precision we have a good understanding of our Earth. However, there is a potential to learn more about our planet from geoneutrinos: and we should take this chance and invest in the next generation of the experiments providing new more precise results.

For an interested reader, more comprehensive information about geoenutrinos can be found in dedicated review articles, as for example [19, 20, 21].

# References


[1] O. Šrámek *et al.*, Earth and Plan. Sci. Let. **361** 356 (2013).

[2] J.H. Davies and D.R. Davies, Solid Earth **1** 5 (2010).

[3] C. Jaupart, S. Labrosse, and J.C. Mareschal, in: D.J. Stevenson (Ed.) Treatise of Geophysics, Elsevier, Amsterdam, pp. 1-53, 2007.

[4] Y. Huang et al., Geochem. Geophys. Geosys. **14** 2003 (2013).

[5] S. Enomoto, E. Ohtani, K. Inoue, and A. Suzuki, Earth Plan. Sci. Lett **258** 147 (2007).

[6] T. Araki *et al.* (KamLAND Collaboration), Nature **436** 499 (2005).

[7] A. Gando *et al.* (KamLAND Collaboration), Nature Geosc. **4** 647 (2011).

[8] A. Gando *et al.* (KamLAND Collaboration), Phys. Rev. D **88** 033001 (2013).

[9] G. Bellini *et al.* (Borexino Collaboration), Phys. Lett. B **687** 299 (2010).

[10] G. Bellini *et al.* (Borexino Collaboration), Phys. Lett. B **722** 295 (2013).

[11] M. Agostini *et al.* (Borexino Collaboration), Phys. Rev. D **92** 031101 (R) (2015).

[12] S. Abe *et al.* (KamLAND Collaboration), Phys. Rev. Lett. **100** 221803 (2008).

[13] G. Bellini *et al.* (Borexino Collaboration), Phys. Rev. D **89** 112007 (2014).

[14] G. Fiorentini *et al.*, Phys. Rev. D **72** 033017 (2005).

[15] M. Coltorti *et al.*, Geochim. Cosmochim. Acta **75** 2271 (2011).

[16] V. Strati *et al.*, Progress in Earth and Planetary Science **2** 5 (2015).

[17] F. An *et al.* (JUNO Collaboration), J. Phys. G: Nucl. Part. Phys. **43** 030401 (2016).

[18] J.G. Learned, S.T. Dye and S. Pakvasa, arXiv: 0810.4975 (2008).

[19] G. Bellini *et al.*, Prog. Part. Nucl. Phys. **73** 1 (2013).

[20] L. Ludhova and S. Zavaterlli, Adv. High En. Phys. **2013** 425693 (2013).

[21] S.T. Dye, Earth Planet. Sci. Lett. **297** 1 (2010).